

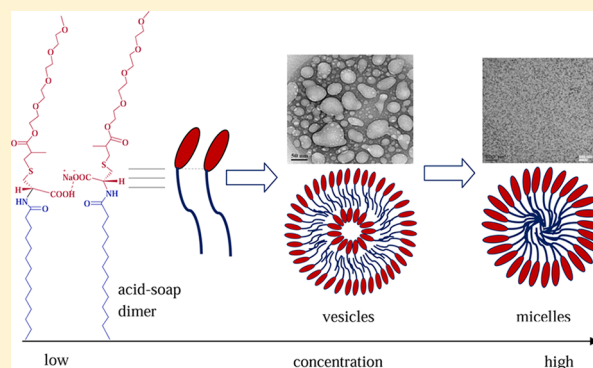
Vesicle-to-Micelle Transition in Aqueous Solutions of L-Cysteine-Derived Carboxylate Surfactants Containing Both Hydrocarbon and Poly(ethylene glycol) Tails

Rita Ghosh and Joykrishna Dey*

Department of Chemistry, Indian Institute of Technology, Kharagpur 721 302, India

S Supporting Information

ABSTRACT: In our recent reports, we have shown that when a poly(ethylene glycol) (PEG) chain is covalently linked to any ionic group, the resultant molecule behaves like an amphiphile. Depending upon the nature of ionic head groups, they self-assemble to form micelles or vesicles, in which the PEG chain constitutes the micellar core or vesicle bilayer. In this study, we intend to examine what happens when both hydrocarbon (HC) and PEG chains are attached to a carboxylate head group. Therefore, we have synthesized two novel amphiphiles in which a PEG and a HC chain is covalently linked to L-cysteine. The surface activities and the solution behavior of the sodium salts of these amphiphiles were investigated at neutral pH. The amphiphiles self-organize to form large unilamellar vesicles in dilute solutions, which transformed into small micelles at higher concentrations. The HC chains of the molecules have been shown to constitute the bilayer membrane of the vesicles and core of micelles. In acidic pH, the amphiphiles were found to form large disklike micelles. The thermodynamic parameters of self-assembly formation were also measured by isothermal titration calorimetry. The vesicle and micelle formation was found to be spontaneous and thermodynamically favorable. The thermal stability of the micelles at neutral and acidic pH was studied. The addition of cholesterol was observed to increase the physical stability of vesicles.



1. INTRODUCTION

Amphiphiles containing a poly(ethylene glycol) (PEG) chain have drawn a great attention owing to their widespread applications in chemistry, biology, medicinal fields, and industry.^{5,6} This is because PEG has low toxicity, nonreactivity, flexible structure, and water solubility. For this reason, PEG can be applied as hydrophilic, ionophilic, or stealth-effect units to develop functional materials and drugs.⁷ One of the interesting properties of PEG is the thermal response. It is known to show lower critical solution temperature (LCST) in water leading to phase separation because of the self-assembly upon temperature elevation.⁸ This is in contrast to ionic surfactants, for example, sodium dodecyl sulfate (SDS) that forms micelles at room temperature, but the critical micelle concentration (cmc) becomes higher and the aggregation number changes upon elevation of temperatures.⁹ For a more effective material and drug design, in-depth understanding on the physicochemical properties of PEG is of significance. However, because conventional PEGs are polydisperse macromolecules, the properties of PEG emerge as averages of the monodisperse species with different molecular weights. Also, the properties of PEG are known to depend on the molecular weights.¹⁰ Recently, the molecular topology has also been found to influence the properties of PEG.¹¹

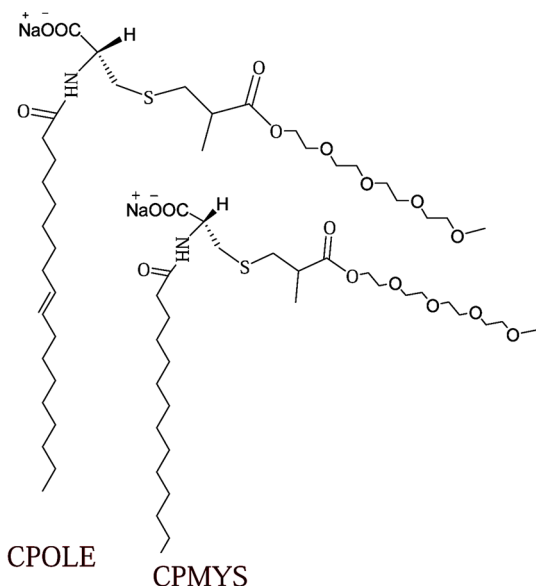
In the past few decades, research on PEG chains have shown that PEG itself acts as a hydrophilic group at room temperature.^{12–15} A number of amphiphilic materials have been developed by coupling the PEG chain with hydrophobic units, such as proteins,^{16–18} cholesterol,^{19,20} and so forth. However, there are also some reports on hydrophobicity of PEG chains, where the PEG chain has been shown to act like the hydrocarbon (HC) tail of conventional surfactants.^{1–4} Therefore, it was thought that when both HC and PEG chains are covalently linked to a polar carboxylate ($-\text{COO}^-$) group, the resulting amphiphilic molecule might behave like a double-tail surfactant. To examine this, we have designed and synthesized two amphiphilic molecules, CPOLE and CPMYS, in which both PEG and HC chains of different lengths are covalently linked to L-cysteine amino acids (see Chart 1 for structures). These amphiphiles may act either like a single-chain or double-chain surfactant depending upon (i) how the PEG chain behaves and (ii) what molecular conformation is adopted in an aqueous medium. Therefore, the aggregation behavior of these amphiphiles was investigated in detail in pH 7.0 buffer at 25 °C using a number of methods. Theoretical calculations

Received: October 22, 2016

Revised: December 7, 2016

Published: December 17, 2016

Chart 1. Chemical Structures of (a) CPOLE and (b) CPMYS



were performed to obtain the stable molecular conformation of the amphiphiles in aqueous solutions. Interfacial properties and cmc of the amphiphiles were analyzed using the surface tension (ST) method. The self-assembly behavior, and micropolarity and microviscosity of the aggregates were measured through the fluorescence probe technique. Dynamic light scattering (DLS) was used to determine the hydrodynamic diameters (d_h) of the aggregates. The morphology of the aggregates was confirmed using transmission electron microscopy (TEM). The thermodynamics of the self-assembly process was studied by isothermal titration calorimetry (ITC). The stability of the aggregates with respect to surfactant concentration, solution pH, temperature, and aging time was studied. The effect of cholesterol on the physical stability of the self-assembled structures formed by these amphiphiles was also investigated.

2. EXPERIMENTAL SECTION

2.1. Materials. Fluorescence probes, *N*-phenyl-1-naphthylamine (NPN), pyrene (Py), and 1,6-diphenyl-1,3,5-hexatriene (DPH) were purchased from Sigma-Aldrich (Bangalore, India) and were recrystallized from acetone–ethanol mixture at least twice before use. Purity of the probes was confirmed by the fluorescence excitation spectra. PEG methyl ether methacrylate (mPEG; MW 300), oleoyl chloride, and myristoyl chloride were purchased from Sigma-Aldrich (Bangalore, India) and were used without any further purification. *L*-Cysteine, sodium bicarbonate, analytical grade sodium dihydrogen phosphate (NaH_2PO_4), and disodium monohydrogen phosphate (Na_2HPO_4) were obtained from SRL (Mumbai, India). Super dry methanol and super dry triethylamine were used for synthesis. Milli-Q water ($18 \text{ M}\Omega \text{ cm}^{-1}$) was used for all aqueous solutions. The amphiphiles, CPOLE and CPMYS were synthesized according to the procedure reported in the literature following Scheme S1. The details are described under “Supporting Information”.

2.2. Methods and Instrumentations. **2.2.1. NMR Measurements.** All 1D (^1H and ^{13}C NMR) and 2D spectra were recorded on a Bruker (600 MHz) NMR spectrometer. The spectra of the acid forms were recorded in CDCl_3 using tetramethylsilane as the internal standard. The 2D nuclear Overhauser effect spectroscopy (NOESY) measurements were taken using a D_2O solvent (Aldrich, 99.6 atom % D) as the chemical shift reference and for mode locking.

2.2.2. Surface Tension Measurements. ST (γ mN/m) measurements were recorded on a GBX 3S (France) surface tensiometer using the Du Nüoy ring detachment method. The instrument was calibrated

and checked by measuring the ST of Milli-Q water ($18 \text{ M}\Omega \text{ cm}^{-1}$) before each experiment. To a 10 mL phosphate buffer (20 mM, pH 7.0) solution, aliquots of the surfactant solution were added, and the resulting mixture was gently stirred and allowed to equilibrate for 10 min before starting the measurement. Each measurement was repeated at least three times until the error was within ± 0.01 mN/m. The temperature of the solution was controlled using a Julabo MC water-circulating bath with a temperature accuracy of ± 0.1 °C.

2.2.3. Steady-State Fluorescence Measurements. The steady-state fluorescence measurements were recorded either on a Perkin-Elmer LS-55 luminescence spectrometer equipped with a temperature-controlled cell holder or on a Horiba FL3-11 spectrophotometer. A Spex Fluorolog-3 (model FL3-11) spectrophotometer was used for recording the fluorescence emission spectra of Py. Surfactant solutions of known concentrations (C_s) were prepared in pH 7.0 buffer (or water) and were incubated for about 30 min before the measurement. For fluorescence titration using an NPN probe, a saturated solution of NPN in pH 7.0 buffer was used. The final concentration of Py and DPH was kept at $1 \mu\text{M}$. Py solutions were excited at 335 nm, and the emission spectra were recorded in the wavelength range of 350–500 nm using excitation and the emission slit widths of 3 and 5 nm, respectively. The solutions containing NPN were excited at 340 nm, and the emission was followed between 350 and 600 nm. The slit width was set at 2.5 nm for excitation and 2.5–10 nm for emission, depending upon the sample concentration. Temperature-controlled measurements were taken using a Thermo Neslab RTE-7 circulating bath.

2.2.4. Fluorescence Anisotropy Measurements. A Perkin-Elmer LS-55 luminescence spectrometer was used to measure the steady-state fluorescence anisotropy (r) of DPH in the presence of the surfactants. The instrument is equipped with a polarization accessory that uses the *L*-format instrumental configuration and a thermostating and magnetically stirred cell housing that allowed temperature control. The anisotropy was calculated using the equation

$$r = (I_{VV} - GI_{VH}) / (I_{VV} + 2GI_{VH}) \quad (1)$$

where I_{VV} and I_{VH} are the fluorescence intensities polarized parallel and perpendicular to the excitation light and $G (=I_{HV}/I_{HH})$ is the instrumental grating factor. The software supplied by the manufacturer automatically determined the G factor and r . For each measurement, the r value was recorded over an integration time of 10 s. For each sample, an average of five readings was accepted as the value of r . A stock solution of 1 mM DPH was prepared in super dry methanol. Aliquots of this stock solution were added to the surfactant solutions, so that the final concentration of the probe was $1 \mu\text{M}$. The anisotropy measurements were taken at different surfactant concentrations in the temperature range of 25–75 °C. Before starting the measurement, each solution was equilibrated for 10 min at the experimental temperature. The sample was excited at 350 nm and the emission intensity was followed at 450 nm using excitation and emission band widths of 2.5 and 2.5–10.0 nm, respectively. A 430 nm cutoff filter was placed in the emission beam to eliminate the effect of the scattered radiation. All measurements were started 30 min after the sample preparation.

2.2.5. Time-Resolved Fluorescence Measurements. An Optical Building Blocks Corporation EasyLife instrument was used to measure the fluorescence lifetime of DPH probes. The light source was a 380 nm diode laser. The time-resolved decay curves were analyzed using a single exponential or biexponential iterative fitting program. The best fit was judged by the χ^2 value (0.8–1.2) and by the randomness of the residual plot.

2.2.6. Determination of Microviscosity. The rigidity or fluidity of the microenvironment of the self-assemblies was measured by the determination of microviscosity (η_m) using the DPH probe. The microviscosity η_m was calculated from the values of r and rotational correlation time (τ_R) of DPH probes using the Debye–Stokes–Einstein relation²¹

$$\eta_m = kT\tau_R/v_h \quad (2)$$

where v_h is the hydrodynamic volume (313 \AA^3)^{22–24} of the DPH molecule. τ_R was calculated using the Perrin's equation

$$\tau_R = \tau_i(r_o/r - 1)^{-1} \quad (3)$$

where r_o ($=0.362$)²² and τ_i are the steady-state fluorescence anisotropy of DPH in a highly viscous solvent and measured fluorescence lifetime of DPH in the surfactant solution, respectively.

2.2.7. Dynamic Light Scattering Measurements. The DLS measurements were recorded using a Zetasizer Nano ZS (Malvern Instrument Laboratory, Malvern, U.K.) light scattering spectrometer equipped with a He–Ne laser operated at 4 mW ($\lambda_o = 632.8 \text{ nm}$) at 25 °C. The solution was filtered directly into the thoroughly cleaned scattering cell through a Millipore Millex syringe filter (Triton free, $0.22 \text{ }\mu\text{m}$). The sample was allowed to equilibrate inside of the DLS optical system chamber for 10 min before starting the measurement. The scattering intensity was normally measured at $\theta = 173^\circ$ to the incident beam. The data acquisition was carried out for at least 15 counts, and each experiment was repeated thrice.

The surface zeta (ζ) potential of the aggregates was also measured using the same Zetasizer Nano ZS (Malvern Instrument Laboratory, Malvern, U.K.) optical system. The measurements were taken by taking different surfactant concentrations in pH 7.0 at 25 °C. An average of three successive measurements was noted for each sample.

2.2.8. TEM. The morphology of the aggregates was investigated using a high-resolution transmission electron microscope (JEM-2100 HRTEM, Make-JEOL, Japan) operating at an accelerating voltage of 200 kV. A $4 \text{ }\mu\text{L}$ volume of the surfactant solution was dropped on to a 400 mesh carbon-coated copper grid and allowed to stand for 1 min. The excess solution was blotted using a piece of tissue paper, and the grid was air-dried. The specimens were kept in desiccators overnight before the measurement. Each measurement was repeated at least twice to check the reproducibility.

2.2.9. ITC. A microcalorimeter, MicroCal iTC₂₀₀ (USA), was used for thermometric measurements. In a microsyringe of capacity $40 \text{ }\mu\text{L}$, the concentrated surfactant solution (0.5 or 3 mM CPOLE, and 1 or 4 mM CPMYS) were taken and added in multiple stages to pH 7.0 buffer kept in the calorimeter cell of capacity $200 \text{ }\mu\text{L}$ under constant stirring conditions, and the stepwise thermogram of the heats of dilution of the surfactant solution was recorded. The stirring speed was fixed at 400 rpm, and the pH 7.0 buffer was taken in the reference cell. Each run was duplicated to check reproducibility. Enthalpy calculations were carried out with the help of ITC software provided by the manufacturer. All measurements were taken at 25 °C.

3. RESULTS AND DISCUSSIONS

3.1. Surface Activity. Surface activity and the interfacial properties of the amphiphiles were studied by ST measurements in pH 7.0 buffer at 25 °C. Figure 1 shows the plots of γ versus $\log C_s$, which exhibits two break points. This is indicative of change in the morphology of the aggregates with the increase

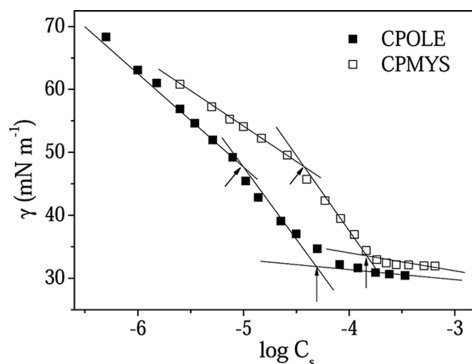


Figure 1. Plots of ST (γ) vs $\log C_s$ in pH 7.0 at 25 °C: (■) CPOLE and (□) CPMYS.

in the surfactant concentration. The surface activity of the amphiphiles can be compared by the minimum ST (γ_{\min}) and pC_{20} [negative log(concentration of surfactant (C_s) at which the γ value of water is reduced by 20 units)] values. For both CPOLE and CPMYS, the γ_{\min} value is approximately 30 mN/m and is similar to that of conventional HC chain surfactants. Also, the pC_{20} values of CPOLE (5.25) and CPMYS (4.84) are higher than those of conventional anionic surfactants, suggesting higher surface activity. Furthermore, the cmc values obtained from the corresponding break points are very low and are similar to those of neutral surfactants.²⁵ This suggests that although there is a $-\text{COO}^-$ group at the head, the PEG chain acts as a stealth making the amphiphiles behave like a neutral surfactant. In other words, the HC chain acts as the tail, and the PEG chain acts as a head group of the amphiphile.

3.2. Self-Assembly Studies. The steady-state fluorescence emission spectrum of NPN is known to exhibit a large blue shift accompanied by a concomitant increase in intensity in going from a polar to nonpolar environment. Therefore, NPN has been extensively used as a hydrophobic probe to study the self-assembly behavior of surfactants. In fact, fluorescence titration using NPN probes is widely used for the determination of cmc of the surfactants and micropolarity of the aggregates.²⁶ Therefore, the fluorescence emission spectra of NPN were recorded in the absence and presence of varying concentrations of both amphiphiles. Not only the fluorescence spectrum shifts toward the shorter wavelength relative to that in water but also the fluorescence intensity increases with the increase in C_s , as shown in Figure S9. This is due to partitioning of the probe molecules into relatively less polar microenvironment and indicates self-assembly formation by the amphiphiles. The plots of spectral shift ($\Delta\lambda$) of the emission maximum relative to those in water ($\Delta\lambda = \lambda_{\text{water}} - \lambda_{\text{surfactant}}$) as a function of C_s are shown in Figure 2. The large blue shift of the fluorescence

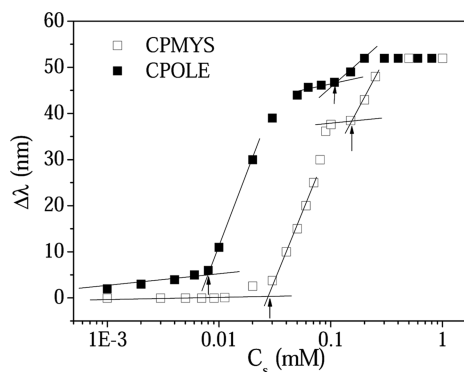


Figure 2. Plots of spectral shift ($\Delta\lambda$) of NPN as a function of surfactant concentration (C_s) in pH 7.0 at 25 °C: (■) CPOLE and (□) CPMYS.

spectrum suggests that the NPN molecules are solubilized within some HC-like environment. The feature of the plots of CPOLE and CPMYS shows two distinct inflections in the sigmoid curve, indicating the existence of two overlapping equilibrium processes in the concentration range used. This is consistent with the existence of two break points in the ST plots and suggests the existence of two types of aggregates in the buffered solution of the surfactants above a critical concentration. The concentrations corresponding to the inflection points were taken as the cmc values and are included in Table 1. It is observed that the cmc values obtained by

Table 1. Self-Assembly Properties of CPOLE and CPMYS Surfactants in Aqueous Solutions of pH 7.0 and 3.0 at 25 °C

pH	surfactant	cmc (μM)		I_1/I_3	η_m	d_h (nm)
		ST	fluorescence			
7.0	CPOLE	10 \pm 10	10 \pm 10	1.02 \pm 0.02 ^a	22.3 \pm 3.0 ^a	5.5 ^a
		100 \pm 30	110 \pm 15			
	CPMYS	37 \pm 10	28 \pm 10	1.02 \pm 0.03 ^b	25.8 \pm 5.0 ^b	10.5 ^b
3.0	CPOLE	150 \pm 50	160 \pm 30	1.05 \pm 0.01 ^a	45.2 \pm 4 ^a	30 ^a
	CPMYS		8 \pm 2	1.06 \pm 0.01 ^b	56.3 \pm 5 ^b	40 ^b

^a[CPOLE] = 2 mM. ^b[CPMYS] = 2 mM.

Table 2. cmc, Standard Gibbs Energy Change (ΔG_m°), Standard Enthalpy Change (ΔH_m°), and Standard Entropy Change (ΔS_m°) of Vesicle/Micelle Formation in Aqueous-Buffered Solution (pH 7.0) by CPOLE and CPMYS at 25 °C

surfactant	cmc ₁ (μM)	cmc ₂ (μM)	ΔH_1 (kJ/mol)	ΔH_2 (kJ/mol)	ΔG_1 (kJ/mol)	ΔG_2 (kJ/mol)	ΔS_1 (J K ⁻¹ /mol)	ΔS_2 (J K ⁻¹ /mol)
CPOLE	20 (\pm 10)	160 (\pm 40)	-1.13 (\pm 0.10)	+0.42 (\pm 0.06)	-48.25	-38.98	+158	+132
CPMYS	37 (\pm 20)	200 (\pm 40)	-0.61 (\pm 0.09)	+1.78 (\pm 0.07)	-44.74	-37.56	+149	+131

fluorescence titration are closer to the respective value obtained by ST measurements.

3.3. Thermodynamics of Self-Assembly Formation.

Generally, thermodynamic parameters are calculated to conjecture the mechanism of self-assembly formation. As the ITC method involves a stepwise addition mode, it provides an excellent procedure to evaluate all thermodynamic parameters in a single run. Therefore, all thermodynamic parameters of the surfactants were evaluated by ITC measurements. In the present study, the thermodynamic parameters were determined by ITC at 25 °C using 0.5 or 3 mM stock solution of CPOLE and 1 or 4 mM stock solution of CPMYS. The ITC thermograms of the amphiphiles at both lower and higher stock concentrations are depicted in Figure S8. The plots show a sigmoid increase in enthalpy with the increase in C_s . The thermodynamic parameters obtained from the plots are included in Table 2. The cmc values of the amphiphiles were obtained from the inflection point of the respective plot. ITC measurements also suggest the existence of two aggregation processes for both CPOLE and CPMYS in the concentration range used. The cmc values thus obtained are close to the corresponding value obtained by ST measurements and fluorimetric titrations. The ΔH_m° value was obtained by subtracting the initial enthalpy from the final enthalpy indicated by the vertical arrow in each plot of Figure S10. Basically, the enthalpy levels between nonmicellar and micellar regions give a measure of the enthalpy of micellization.²⁷ The ΔG_m° value was calculated from the measured cmc value using the following relationship²⁸

$$\Delta G_m^\circ = (1 + \beta)RT \ln(a_{\text{cmc}}) \quad (4)$$

where β is the degree of counterion binding of the surfactant molecule and is usually taken as 0.8 for anionic surfactants²⁹ and a_{cmc} is the activity of the surfactant solution at cmc, which is numerically equal to the value of cmc as the solution is very dilute. The ΔS_m° value was evaluated by the Gibbs equation

$$\Delta S_m^\circ = (\Delta H_m^\circ - \Delta G_m^\circ)/T \quad (5)$$

The spontaneity of vesicle formation is suggested by the very large negative and positive values of ΔG_m° and ΔS_m° , respectively. The very large negative values of ΔG_m° also indicate that the transition between the two types of aggregates at high surfactant concentrations is spontaneous but less favored in comparison with the vesicle formation in dilute

solutions. Furthermore, the $T\Delta S_m^\circ$ values for all surfactants are found to be much larger than the ΔH_m° values, which means spontaneous aggregate formation is an entropy-driven process. This means that the driving force for aggregation is an hydrophobic interaction.²⁹ The release of water molecules around the HC tails contributes to the entropy rise facilitating the self-assembly process. This suggests that the aggregation process of the two surfactant systems is similar to most HC tail surfactants. The thermodynamic parameters of the surfactants demonstrate that the aggregate formation is much more feasible and spontaneous when compared not only with conventional ionic surfactants with a HC tail but also with those with only a PEG tail.^{3,4} This must be a result of the reduction of ionic repulsion among $-\text{COO}^-$ groups owing to the stealth properties of the PEG chains on the surface.

3.4. Hydrodynamic Size of Aggregates. To investigate the structural transition in surfactant solutions, DLS measurements were taken to measure the hydrodynamic diameter (d_h) of the aggregates at different concentrations of the surfactants. The size distribution histograms of the aggregates are shown in Figure 3. In dilute solutions, a monomodal distribution with a large mean d_h value of ~ 60 nm for CPOLE and ~ 250 nm for CPMYS is observed, suggesting the existence of large

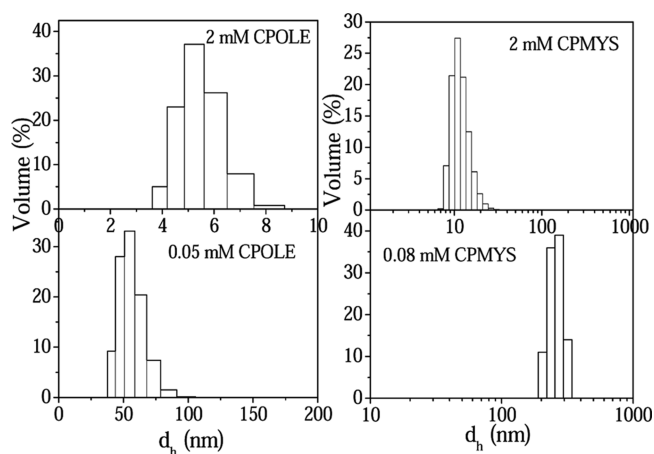


Figure 3. Size distribution histograms of CPOLE in solutions of pH 7.0 with $C_s = 0.05$ and 2.0 mM and of CPMYS with $C_s = 0.08$ and 2.0 mM at 25 °C.

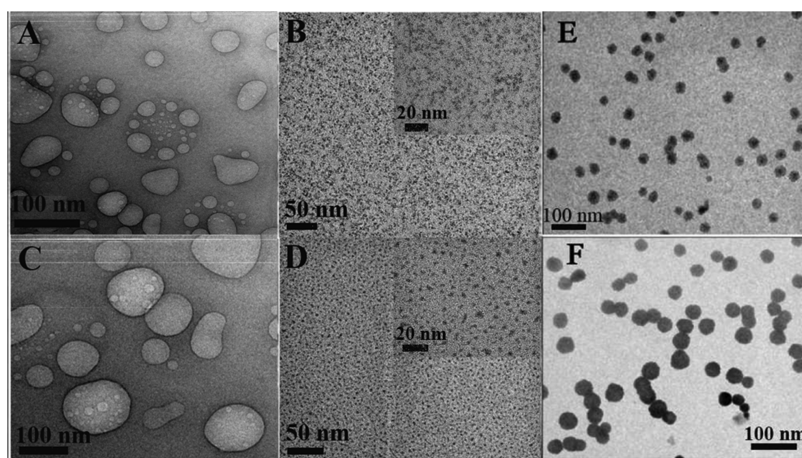


Figure 4. HRTEM micrographs of (A) 0.05 mM CPOLE, (B) 3 mM CPOLE (inset: enlarged image), (C) 0.08 mM CPMYS, (D) 3 mM CPMYS (inset: enlarged image) in pH 7.0 buffer, and (E) and (F) 2 mM CPOLE and 2 mM CPMYS, respectively, at pH 3.0.

aggregates. On the other hand, the monomodal size distribution with a smaller mean d_h value of ~ 5 nm for CPOLE and ~ 10 nm for CPMYS in moderately concentrated solutions clearly indicate the existence of small micelles. This means that both CPOLE and CPMYS surfactants produce larger aggregates at lower concentrations, which transform into much smaller micelle-like aggregates upon increase in the surfactant concentration. To determine the morphology of the aggregates, we have performed TEM measurements in both dilute and concentrated solutions of CPOLE and CPMYS as discussed below.

3.5. Morphology of Aggregates. To visualize the microstructures formed by the surfactants, HRTEM measurements were taken at different concentrations of the surfactants at pH 7.0. The micrographs obtained without negative staining of the specimens are shown in Figure 4. Large-closed spherical vesicles can be observed in dilute aqueous solutions of both surfactants. However, at higher surfactant concentrations, only small micelle-like microstructures are found in the case of CPOLE and CPMYS. It should be noted that although the sample preparation involved drying, the results were reproducible. However, negatively stained (with 1% phosphotungstic acid, pH 7.0) specimens showed only large and elongated micelle-like aggregates (see Figure S11). This is probably due to increased counterion condensation in the presence of sodium salts leading to the formation of elongated micelles. Although because of low resolution, we are unable to comment on the exact number of lamellas of the vesicles, they appear to have a thin boundary corresponding to unilamellar vesicles (ULVs). The deformation observed in the vesicular structure could be due to the fusion of smaller vesicles facilitated by the exchange of amphiphiles between two interacting vesicles. As a result, the vesicles are polydisperse (which is normal with spontaneously formed vesicles) in size with d_h values in the range of 50–200 nm. However, the results are consistent with those of DLS measurements. The existence of small aggregates (micrographs B and D) in concentrated surfactant solutions is also consistent with the results of DLS measurements.

3.6. Surface Charge of Aggregates. The stability of colloidal particles is determined by a ζ -potential value, which is a measure of its surface charge. In fact, ζ -potential is a measure of the degree of repulsion between the adjacent and the like-charged particles in dispersion. A high ζ -potential value (positive or negative) is indicative of the stability of the system

against flocculation or coagulation. Therefore, ζ -potential values of the vesicles or micelles formed by the surfactants were measured in different pHs at different concentrations. The data are listed in Table S1. Relatively low ζ values are expected for the $-\text{COO}^-$ surfactants, as the salts hydrolyze in dilute solutions to produce their corresponding acid form, facilitating the formation of an acid–soap dimer. Thus, lower values of ζ -potential in dilute solutions mean stronger intermolecular attraction among the surfactant molecules in the aggregates, allowing the molecules to pack tightly thereby producing large vesicular aggregates. On the other hand, higher ζ -potential values in the concentrated solution mean greater repulsion among the head groups and hence the formation of smaller aggregates. The very low ζ -potential values for the aggregates of both surfactants at pH 3.0 suggest the formation of uncharged micelles due to the conversion of soap to an acid form of the amphiphile, as discussed below.

3.7. Vesicle-to-Micelle Transition. From the above discussion, it can be concluded that the first cmc (cmc_1) corresponds to vesicle formation and therefore it can be referred to as critical vesicle concentration (cvc). On the other hand, the second cmc (cmc_2) is actually the critical concentration for the vesicle-to-micelle phase transition. Several mechanisms of vesicle-to-micelle transition, including monomer diffusion and fusion of vesicles have been suggested.^{30,31} The vesicles have a dynamic structure between the monomers and the vesicles. Actually in dilute solutions of the amphiphiles at pH 7.0, hydrolysis of the salt form of the surfactant produces its acid form. When their concentrations are equal, they interact through hydrogen bonding and thus produce acid–soap dimers. Because the electrostatic repulsion between the head groups is eliminated, the acid–soap dimers self-organize to produce large aggregates-like bilayer vesicles. Such behavior of the surfactants is quite similar to the medium- and long-chain fatty acid salts.^{32–35} However, at higher surfactant concentrations, due to the decrease in the degree of hydrolysis, the $-\text{COO}^-$ form predominates. This results in an increase in electrostatic repulsion among the surfactant molecules triggering the reorganization of vesicle bilayers to form smaller aggregates-like spherical micelles.

According to the results of fluorescence probe studies, the HC chain of the amphiphiles constitutes the bilayer membrane of vesicles at low concentrations and the core of micelles at higher concentrations. The spatial arrangement of the

surfactant molecules in the aggregated state was further inferred from the 2D NOESY spectra (Figure S12) of CPOLE, as a representative example. Such experiments have been shown to give excellent insights into the nature of interactions in the self-assembly process in a number of aggregated systems.^{36–38} As the *cvc* values of the amphiphiles are very low, it was difficult to record the NOESY spectra in the vesicular state of the surfactant. Therefore, a 2D NOESY spectrum was recorded in D₂O at the micellar state of CPOLE at $C_s = 2$ mM. From the NOESY spectrum (Figure S12), it is clear that there are mainly diagonal interactions along with some key cross interactions, which imply that the only interactions between the adjacent H atoms in the PEG chain and HC chain were observed. In other words, only intra- and intermolecular interactions among the PEG chains and HC chains were observed for CPOLE in their aggregated state. Thus, the spatial interactions of the H atoms indicate the micelle-like aggregate formation for CPOLE at higher concentrations.

3.8. Microenvironment of the Aggregates. The micropolarity of the self-assemblies was measured using Py as the fluorescent probe. The intensities of the vibronic bands of the Py fluorescence spectrum are found to depend strongly on the solvent polarity.³⁹ More specifically, the ratio (I_1/I_3) of the intensities of the first (I_1 , 372 nm) to the third (I_3 , 384 nm) vibronic bands in the fluorescence spectrum of Py is very sensitive to solvent polarity change, and therefore, it is used as the micropolarity index.³⁹ The fluorescence spectra of Py in the presence of different concentration surfactants are depicted in Figure S13. The I_1/I_3 values (Table 1) for CPOLE (2 mM) and CPMYS (2 mM) are very low compared with those in water (1.82). This means that Py is solubilized within the hydrophobic microdomains of self-assemblies consisted only of the HC tails.³⁹ Such a highly nonpolar microenvironment is consistent with the formation of aggregates consisting only of the HC tails.⁴⁰ Moreover, the I_1/I_3 values, within the limit of experimental error, are almost equal for CPOLE and CPMYS. This is because Py is solubilized deep into the HC region of the aggregates. It is interesting to note that the I_1/I_3 values of CPOLE and CPMYS are much less than those of the conventional HC tail surfactants. This means that the HC tails of the surfactant molecules in the aggregates are tightly packed, and as a result, the degree of water penetration is very low. These results thus indicate that such self-assembled structures will be useful for the solubilization of hydrophobic drugs.

To further estimate the rigidity of the microenvironment of the aggregates formed by the surfactants, we have performed steady-state fluorescence anisotropy (r) measurements using DPH as a probe molecule. The fluorescence spectra as shown in Figure S14 indicate the gradual incorporation of DPH molecules within the microenvironment of the aggregates and is consistent with the results of fluorescence titration carried out using the NPN probe. The fluorescence anisotropy r is an index of microfluidity (or microviscosity) of the vesicle membrane or micelle core. In fact, DPH is a widely used probe for the study of both static and dynamic properties of membranes, such as membrane fluidity and ordering of lipid acyl chains.^{41,42} Therefore, the r value of DPH was measured at different concentrations of the surfactants above their *cvc* values in pH 7.0 buffer at 25 °C. The plots in Figure 5 show that the r value is very high at low concentrations of both surfactants, which decreases to a large extent with the increase in C_s . The higher value of r at low concentrations implies an

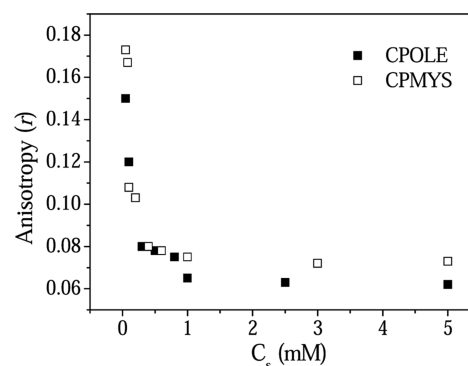


Figure 5. Plots of fluorescence anisotropy (r) of DPH vs surfactant concentration (C_s) at 25 °C: (■) CPOLE and (□) CPMYS.

ordered environment around the DPH probe in the self-assemblies and thus supports the existence of bilayer vesicles in dilute solutions of the amphiphiles. However, the smaller value of r at higher surfactant concentrations suggests the existence of loosely packed self-assemblies, such as micelles.⁴³ The decrease in the steady-state r value of DPH probes clearly indicates that the vesicles with a rigid bilayer membrane are transformed into small micelles with the increase in surfactant concentration.

To quantify the rigidity of the microenvironments of the aggregates, we have also determined η_m around the DPH probe within the aggregates. The η_m value was calculated from the measured r value and fluorescence lifetime (τ_f) of the DPH probe in the presence of surfactants according to a reported method,⁴⁴ which is briefly described under Supporting Information. The τ_f values (Table S2) were obtained from the analysis of fluorescence intensity decays of the DPH probe in the presence of surfactants at pH 7.0. The η_m values thus obtained are included in Table 1. The η_m values of the concentrated (2 mM) CPOLE and CPMYS is 22.3 and 25.8 mPa s⁻¹, respectively, which are similar to those of the micellar aggregates of SDS and dodecyltrimethylammonium bromide surfactants.⁴⁴ However, at low surfactant concentrations, for example, in 0.08 mM CPOLE (49.6 mPa s⁻¹) and 0.1 mM CPMYS (55.8 mPa s⁻¹) the η_m values of the self-assemblies are relatively higher, which is indicative of the formation of closed bilayer vesicles as already suggested by the TEM pictures (Figure 4).

3.9. Effect of pH. The surfactants being sodium salts of carboxylic acids, it is expected that the change in pH will have an effect on the aggregation behavior of the amphiphiles. This is because the pH-induced protonation of the $-\text{COO}^-$ group affects the hydrophilic interaction between the head groups of the ionic surfactants and hence will have a defining effect on the *cvc* value and on the shape and size of the aggregates formed by the surfactant molecules. The cmc values of the surfactants were therefore measured at pH 3.0 using NPN as a fluorescent probe. The fluorescence titration curves are shown in Figure 6. It is interesting to note that the plots exhibit only one inflection point. The cmc values obtained from the concentration corresponding to the inflection point are found to be much less than the *cvc* value obtained at neutral pH. This is expected because at pH 3.0 the $-\text{COO}^-$ group being protonated, the surfactant molecule exists mainly in the neutral form. Thus, as a result of elimination of charge repulsion among the head groups, the cmc value decreased for both surfactants (Table 1). As can be seen from the fluorescence titration curves, the fluorescence spectrum of NPN is highly blue-shifted relative to

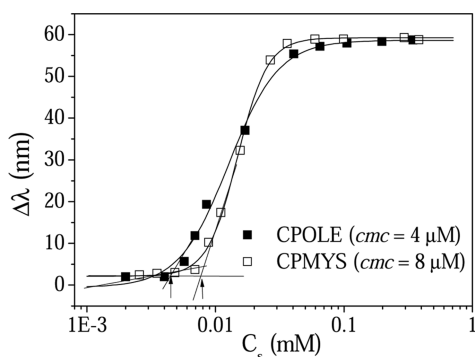


Figure 6. Plots of spectral shift ($\Delta\lambda$) of NPN as a function of surfactant concentration (C_s) in pH 3.0 at 25 °C: (■) CPOLE and (□) CPMYS.

that in water, suggesting that the micelles have a HC-like micellar core.

The effect of the pH on the microenvironment was monitored by measuring the I_1/I_3 ratio of Py. The data in Table 1 show that the micelles in pH 3.0 have micropolarity-like HC solvents. The rigidity of the microenvironment was monitored by fluorescence anisotropy of DPH. The representative plots of the variation in r as a function of pH are shown in Figure 7. The sigmoidal plots clearly indicate the existence of

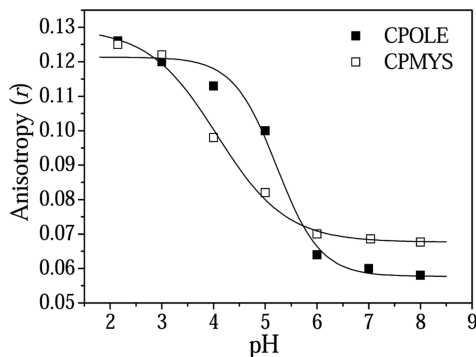


Figure 7. Plots of fluorescence anisotropy (r) of DPH in (■) 2 mM CPOLE and (□) 2 mM CPMYS as a function of pH.

a two-state equilibrium between the $-\text{COO}^-$ and $-\text{COOH}$ forms of the surfactant molecule. The pK_a values thus obtained from the inflection points of the plots are approximately 5.5 and 4.5 for CPOLE and CPMYS, respectively. This suggests that at pH 3.0, both surfactant molecules are present mostly in the neutral carboxylic acid form. This means the reduction of electrostatic repulsion between the head groups and hence tight packing of the surfactant monomers in the aggregates at $\text{pH} \leq 3$, as indicated by the higher η_m value (Table 1) of the micelles.

The tight packing of the charge neutral surfactant monomers in the aggregates as discussed above will result in the growth of micelles at low pH. Therefore, we measured the hydrodynamic diameter of the micelles of both surfactants at different pHs. The size distribution histograms can be found in Figure 8. It is observed that the mean d_h value increased relative to that in neutral pH. This suggests the formation of larger micelles in acidic pH, which is confirmed by the HRTEM images of the surfactant solutions at pH 3.0. Indeed, both micrographs (E) and (F) in Figure 4 exhibit large disklike micelles for CPOLE and CPMYS surfactants.

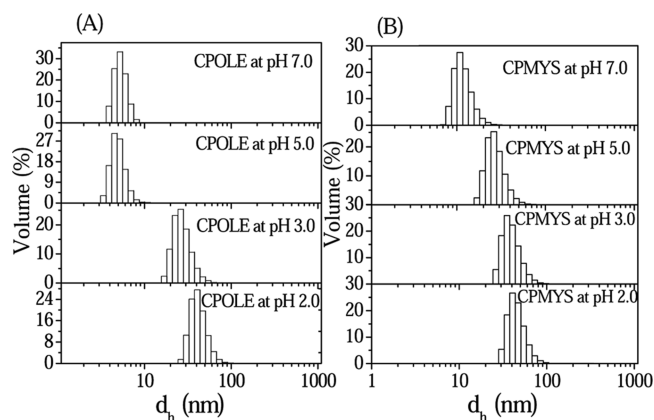


Figure 8. Size distribution histograms of (A) 2 mM CPOLE and (B) 2 mM CPMYS at different pHs.

3.10. Effect of Temperature. Temperature is a physiological parameter in colloidal chemistry. It is well-known that PEG chain-containing neutral surfactants or polymers undergo dehydration at higher temperatures and fall out of solution showing appearance of turbidity.⁴⁵ The critical temperature above which this occurs is called LCST. However, the surfactant solutions at pH 7.0 did not exhibit any LCST phenomena in the concentration range (0.05–2 mM) studied as shown by the plots in the inset of Figure 9. The study thus

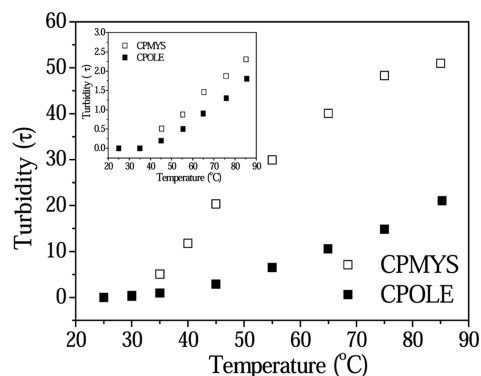


Figure 9. Plots of turbidity (τ) as a function of temperature ($^{\circ}\text{C}$) of the surfactant solutions (0.5 mM) at pH 3.0: (■) CPOLE and (□) CPMYS (inset: turbidity plots at pH 7.0).

demonstrates that the aggregates of CPOLE and CPMYS surfactants are stable at the physiological pH and temperature (37 °C). By contrast, surfactant solutions (0.05 mM) of both surfactants at pH 3.0 exhibit LCST phenomena. Therefore, temperature variation turbidity ($\tau = 100 - \%T$) was measured with surfactant solutions (0.5 mM) at a concentration much above their cmc values at pH 3.0. As can be seen in Figure 9, CPMYS exhibits $\sim 50\%$ turbidity upon elevation of temperatures to 85 °C. The LCST value appears to be ~ 43 °C. The LCST value, however, is found to be less at higher concentrations of CPMYS. On the other hand, for CPOLE, the turbidity of 0.05 mM solution was found to be less ($< 20\%$) at the highest achievable temperature (85 °C) in water and the LCST is observed to be ~ 55 °C. This suggests that the nonionic CPMYS (at pH 3.0) may have potential applications in the field of drug delivery for hydrophobic therapeutic agents.

3.11. Effect of Cholesterol. Cholesterol (Chol) is a major component of biological membrane lipids and is known to

control the membrane fluidity, diffusional mobility, and permeability.⁴⁶ The intravesicle interactions of Chol are hydrophobic, hydrophilic, and steric interactions that determine the molecular order and membrane properties.^{47–50} As mentioned earlier, the ULVs get deformed as a result of fusion with each other because of the exchange of surfactant molecules. Therefore, to enhance the stability of vesicles in dilute solutions, we studied the effect of the addition of Chol. Usually, there is an upper limit to Chol incorporation within the aggregate, above which Chol seems to precipitate as crystals of pure Chol either in the monohydrate or in the anhydrous form. In fact, the solubility of Chol in the vesicle bilayer was found to be very low (~ 2 mol %) in 0.08 mM surfactant solution. In the presence of 2% Chol, the r value of DPH probes was observed to increase from 0.162 to 0.263 for CPOLE and from 0.175 to 0.282 for CPMYS (Figure S16), indicating the increase in bilayer rigidity and hence physical stability of the vesicles.

3.12. Aging Effect. It should be noted that the PEG chain covalently attached to the surfactant head group contains a hydrolyzable ester linkage. The hydrolysis of the surfactant could destabilize the vesicles or micelles at room temperature even at neutral pH. Therefore, it is important to determine the shelf-life of the micelles formed by the surfactants in neutral pH at room temperature. To determine the stability of colloidal formulation, the turbidity ($\tau = 100 - \%T$) of the surfactant solution was measured at different time intervals. Turbidity, generally, arises from the scattering of light by the aggregates and depends on their sizes and populations. The turbidity of 0.05 and 0.5 mM CPOLE and 0.08 and 0.5 mM CPMYS solutions in pH 7.0 buffer (20 mM) was monitored at 400 nm at different time intervals during 30 days. The results are summarized in Figure S17. It is important to note that in the concentration range used, turbidity remains almost constant at $\leq 10\%$ throughout the aging period, showing good storage life of the vesicles and micelles.

4. CONCLUSIONS

In summary, two anionic surfactants CPOLE and CPMYS containing both PEG and HC chains were designed, synthesized, and characterized. Both surfactants exhibit very good surface activity in pH 7.0 buffer at 25 °C. The surfactants were observed to self-organize spontaneously to form ULVs in very dilute solutions. However, the vesicles are transformed into micelles upon the increase in the surfactant concentration. The cmc values for the vesicle and micelle formation are relatively low. The thermodynamic data suggest that both vesicles and micelles are formed spontaneously in solution above a relatively low cmc value. The large positive values of ΔS_m° indicate that the driving force behind the spontaneous vesicle/micelle formation is an hydrophobic interaction. The microenvironments of both vesicles and micelles were observed to be much less compared with bulk water, suggesting that the vesicle bilayer and the micelle core are constituted by the HC chains of the surfactant molecules. This means that the PEG chains are directed either toward aqueous core of the bilayer vesicles or toward bulk water. At a pH below their pK_a value, both surfactants form large disklike micelles above a very low critical concentration ($cmc \approx 5 \mu M$). The vesicles and micelles were observed to be stable in the temperature range of 20–75 °C at pH 7.0 over a long period of time. However, at pH 3.0, micelles of CPMYS surfactants exhibit LCST at a temperature of about 43 °C as a result of temperature-induced dehydration

of the PEG chains. The ULVs formed in dilute solutions of CPOLE and CPMYS become more stable upon the addition of cholesterol as an additive. Despite having ester linkage in the molecular structure of the surfactants, the ULVs of both surfactants were found to be stable at pH 7.0 for more than 30 days. Therefore, the ULVs can have potential applications in drug delivery.

■ ASSOCIATED CONTENT

📄 Supporting Information

The Supporting Information is available free of charge on the ACS Publications website at DOI: 10.1021/acs.langmuir.6b03845.

Details of synthetic procedure, FT-IR, ¹H NMR, and ¹³C NMR spectra and chemical identification of the synthesized amphiphiles, experimental methods, ITC plots, representative fluorescence emission spectra of NPN, DPH, and Py, 2D NOESY spectrum, curcumin absorption and emission spectra, and tables of fluorescence lifetime and ζ -potential values (PDF)

■ AUTHOR INFORMATION

Corresponding Author

*E-mail: joydey@chem.iitkgp.ernet.in. Fax: (+)91-3222-255303.

Notes

The authors declare no competing financial interest.

■ ACKNOWLEDGMENTS

The authors thank the Indian Institute of Technology, Kharagpur for financial support of this work. We are thankful to Prof. D. Dhara for the DLS and ζ -potential measurements.

■ REFERENCES

- (1) Dey, J.; Shrivastava, S. Can Molecules with Anionic Head and Poly(ethylene glycol) Methyl Ether Tail Self-Assemble in Water? A Surface Tension, Fluorescence Probe, Light Scattering, and Transmission Electron Microscopic Investigation. *Soft Matter* **2012**, *8*, 1305–1308.
- (2) Dey, J.; Shrivastava, S. Physicochemical Characterization and Self-Assembly Studies on Cationic Surfactants Bearing mPEG Tail. *Langmuir* **2012**, *28*, 17247–17255.
- (3) Ghosh, R.; Dey, J. Vesicle Formation by L-Cysteine-Derived Unconventional Single-Tailed Amphiphiles in Water: A Fluorescence, Microscopy, and Calorimetric Investigation. *Langmuir* **2014**, *30*, 13516–13524.
- (4) Ghosh, R.; Dey, J. Aggregation Behavior of Poly(ethylene glycol) Chain-Containing Anionic Amphiphiles: Thermodynamic, Spectroscopic and Microscopic Studies. *J. Colloid Interface Sci.* **2015**, *451*, 53–62.
- (5) Elbert, D. L.; Hubbell, J. A. Surface Treatments of Polymers for Biocompatibility. *Annu. Rev. Mater. Sci.* **1996**, *26*, 365–394.
- (6) Dhawan, S.; Dhawan, K.; Varma, M.; Sinha, V. R. Applications of Poly(ethylene oxide) in Drug Delivery Systems. Part II. *Pharm. Technol.* **2005**, *29*, 82–96.
- (7) Harris, J. M. *Poly(ethylene glycol) Chemistry: Biotechnical and Biomedical Applications in Topics in Applied Chemistry*; Plenum Press: New York, 1992.
- (8) Saeki, N.; Kuwahara, N.; Nakata, M.; Kaneko, M. Upper and Lower Critical Solution Temperatures in Poly(ethylene glycol) Solutions. *Polymer* **1976**, *17*, 685–689.
- (9) Bezzobotnov, V. Y.; Borbely, S.; Cser, L.; Farago, B.; Gladkih, I. A.; Ostanevich, Y. M.; Vass, S. Temperature and Concentration Dependence of Properties of Sodium Dodecyl Sulfate Micelles

Determined from Small Angle Neutron Scattering Experiments. *J. Phys. Chem.* **1988**, *92*, 5738–5743.

(10) Chen, Y.; Dong, C.-M. pH-Sensitive Supramolecular Polypeptide-Based Micelles and Reverse Micelles Mediated by Hydrogen-Bonding Interactions or Host–Guest Chemistry: Characterization and in Vitro Controlled Drug Release. *J. Phys. Chem. B* **2010**, *114*, 7461–7468.

(11) Muraoka, T.; Adachi, K.; Ui, M.; Kawasaki, S.; Sadhukhan, N.; Obara, H.; Tochio, H.; Shirakawa, M.; Kinbara, K. A Structured Monodisperse PEG for the Effective Suppression of Protein Aggregation. *Angew. Chem., Int. Ed.* **2013**, *52*, 2430–2434.

(12) Carstens, M. G.; van Nostrum, C. F.; Ramzi, A.; Meeldijk, J. D.; Verrijck, R.; de Leede, L. L.; Crommelin, D. J. A.; Hennink, W. E. Poly(ethylene glycol)–Oligolactates with Monodisperse Hydrophobic Blocks: Preparation, Characterization, and Behavior in Water. *Langmuir* **2005**, *21*, 11446–11454.

(13) Park, M.-J.; Chung, Y.-C.; Chun, B. C. PEG-Based Surfactants that Show High Selectivity in Disrupting Vesicular Membrane with or without Cholesterol. *Colloids Surf., B* **2003**, *32*, 11–18.

(14) Salonen, A.; Knyazev, A.; von Bandel, N.; Degrouard, J.; Langevin, D.; Drenckhan, W. A Novel Pyrene-Based Fluorescing Amphiphile with Unusual Bulk and Interfacial Properties. *ChemPhysChem* **2011**, *12*, 150–160.

(15) Mandal, A. B.; Ray, S.; Biswas, A. M.; Moulik, S. P. Physicochemical Studies on the Characterization of Triton X 100 Micelles in an Aqueous Environment and in the Presence of Additives. *J. Phys. Chem.* **1980**, *84*, 856–859.

(16) Zalipsky, S. Chemistry of Polyethylene Glycol Conjugates with Biologically Active Molecules. *Adv. Drug Delivery Rev.* **1995**, *16*, 157–182.

(17) Veronese, F. M. Peptide and Protein PEGylation: A Review of Problems and Solutions. *Biomaterials* **2001**, *22*, 405–417.

(18) Caliceti, P.; Veronese, F. M. Pharmacokinetic and Biodistribution Properties of Poly(ethylene glycol)–Protein Conjugates. *Adv. Drug Delivery Rev.* **2003**, *55*, 1261–1277.

(19) Li, J.; He, Z.; Yu, S.; Li, S.; Ma, Q.; Yu, Y.; Zhang, J.; Li, R.; Zheng, Y.; He, G.; Song, X. Micelles Based on Methoxy Poly(ethylene glycol) Cholesterol Conjugate for Controlled and Targeted Drug Delivery of a Poorly Water Soluble Drug. *J. Biomed. Nanotechnol.* **2012**, *8*, 809–817.

(20) Xu, H.; Wang, K. Q.; Deng, Y. H.; Chen, D. W. Effects of Cleavable PEG-Cholesterol Derivatives on the Accelerated Blood Clearance of PEGylated Liposomes. *Biomaterials* **2010**, *31*, 4757–4763.

(21) Lakowicz, J. R. *Principles of Fluorescence Spectroscopy*; Plenum Press: New York, 1983; p 132.

(22) Shinitzky, M.; Barenholz, Y. Dynamics of the Hydrocarbon Layer in Liposomes of Lecithin and Sphingomyelin Containing Dicetylphosphate. *J. Biol. Chem.* **1974**, *249*, 2652–2657.

(23) Ke, D.; Wang, X.; Yang, Q.; Niu, Y.; Chai, S.; Chen, Z.; An, X.; Shen, W. Spectrometric Study on the Interaction of Dodecyltrimethylammonium Bromide with Curcumin. *Langmuir* **2011**, *27*, 14112–14117.

(24) Zhanga, Z.; Feng, S.-S. The Drug Encapsulation Efficiency, in Vitro Drug Release, Cellular Uptake and Cytotoxicity of Paclitaxel-Loaded Poly(lactide)–Tocopheryl Polyethylene Glycol Succinate Nanoparticles. *Biomaterials* **2006**, *27*, 4025–4033.

(25) Mittal, K. L. Determination of CMC of Polysorbate 20 in Aqueous Solution by Surface Tension Method. *J. Pharm. Sci.* **1972**, *61*, 1334–1335.

(26) Saitoh, T.; Taguchi, K.; Hiraide, M. Evaluation of Hydrophobic Properties of Sodium Dodecylsulfate/ γ -Alumina Admicelles Based on Fluorescence Spectra of *N*-Phenyl-1 Naphthylamine. *Anal. Chim. Acta* **2002**, *454*, 203–208.

(27) Paula, S.; Sues, W.; Tuchtenhagen, J.; Blume, A. Thermodynamics of Micelle Formation as a Function of Temperature: A High Sensitivity Titration Calorimetry Study. *J. Phys. Chem.* **1995**, *99*, 11742–11751.

(28) Verrall, R. E.; Milioto, S.; Zana, R. Ternary Water-in-Oil Microemulsions Consisting of Cationic Surfactants and Aromatic Solvents. *J. Phys. Chem.* **1988**, *92*, 3939–3943.

(29) Majhi, P. R.; Moulik, S. P. Energetics of Micellization: Reassessment by a High-Sensitivity Titration Microcalorimeter. *Langmuir* **1998**, *14*, 3986–3990.

(30) Zhdanov, V. P.; Kasemo, B. Lipid-Diffusion-Limited Kinetics of Vesicle Growth. *Langmuir* **2000**, *16*, 7352.

(31) Ohta, A.; Danev, R.; Nagayama, K.; Mita, T.; Asakawa, T.; Miyagishi, S. Transition from Nanotubes to Micelles with Increasing Concentration in Dilute Aqueous Solution of Potassium *N*-Acyl Phenylalaninate. *Langmuir* **2006**, *22*, 8472–8477.

(32) Gebicki, J. M.; Hicks, M. Ufasomes are Stable Particles Surrounded by Unsaturated Fatty Acid Membranes. *Nature* **1973**, *243*, 232–234.

(33) Namani, T.; Walde, P. From Decanoate Micelles to Decanoic Acid/Dodecylbenzenesulfonate Vesicles. *Langmuir* **2005**, *21*, 6210–6219.

(34) Cistola, D. P.; Hamilton, J. A.; Jackson, D.; Small, D. M. Ionization and Phase Behavior of Fatty Acids in Water: Application of the Gibbs Phase Rule. *Biochemistry* **1988**, *27*, 1881–1888.

(35) Hargreaves, W. R.; Deamer, D. W. Liposomes from Ionic, Single-Chain Amphiphiles. *Biochemistry* **1978**, *17*, 3759–3768.

(36) Neuhaus, D.; Williamson, M. P. *The Nuclear Overhauser Effect in Structural and Conformational Analysis*; Wiley-VCH: New York, 2000.

(37) Yuan, H.-Z.; Cheng, G.-Z.; Zhao, S.; Miao, X.-J.; Yu, J.-Y.; Shen, L.-F.; Du, Y.-R. Conformational Dependence of Triton X-100 on Environment Studied by 2D NOESY and ^1H NMR Relaxation. *Langmuir* **2000**, *16*, 3030–3035.

(38) Denkova, P. S.; Van Lokeren, L.; Verbruggen, I.; Willem, R. Self-Aggregation and Supramolecular Structure Investigations of Triton X-100 and SDP₂S by NOESY and Diffusion Ordered NMR Spectroscopy. *J. Phys. Chem. B* **2008**, *112*, 10935–10941.

(39) Kalyanasundaram, K.; Thomas, J. K. Environmental Effects on Vibronic Band Intensities in Pyrene Monomer Fluorescence and Their Application in Studies of Micellar Systems. *J. Am. Chem. Soc.* **1977**, *99*, 2039–2044.

(40) Kalyanasundaram, K. *Photophysics of Microheterogeneous Systems*; Academic Press: New York, 1988.

(41) Shinitzky, M.; Dianoux, A. C.; Gitler, C.; Weber, G. Microviscosity and Order in the Hydrocarbon Region of Micelles and Membranes Determined with Fluorescent Probes. I. Synthetic Micelles. *Biochemistry* **1971**, *10*, 2106–2113.

(42) Shinitzky, M.; Yuli, I. Lipid Fluidity at the Submacroscopic Level: Determination by Fluorescence Polarization. *Chem. Phys. Lipids* **1982**, *30*, 261–282.

(43) Zana, R.; In, M.; Lévy, H.; Duportail, G. Alkanediyl- α,ω -bis(dimethylalkylammonium bromide). 7. Fluorescence Probing Studies of Micelle Micropolarity and Microviscosity. *Langmuir* **1997**, *13*, 5552–5557.

(44) Roy, S.; Mohanty, A.; Dey, J. Microviscosity of Bilayer Membranes of Some *N*-Acylamino Acid Surfactants Determined by Fluorescence Probe Method. *Chem. Phys. Lett.* **2005**, *414*, 23–27.

(45) Cui, Q.; Wu, F.; Wang, E. Thermosensitive Behavior of Poly(ethylene glycol)-Based Block Copolymer (PEG-*b*-PADMO) Controlled via Self-Assembled Microstructure. *J. Phys. Chem. B* **2011**, *115*, 5913–5922.

(46) Yeagle, P. L. Cholesterol and the Cell Membrane. *Biochim. Biophys. Acta, Biomembr.* **1985**, *822*, 267–287.

(47) Raffy, S.; Teissié, J. Control of Lipid Membrane Stability by Cholesterol Content. *Biophys. J.* **1999**, *76*, 2072–2080.

(48) Harada, T.; Pham, D.-T.; Leung, M. H. M.; Ngo, H. T.; Lincoln, S. F.; Easton, C. J.; Kee, T. W. Cooperative Binding and Stabilization of the Medicinal Pigment Curcumin by Diamide Linked γ -Cyclodextrin Dimers: A Spectroscopic Characterization. *J. Phys. Chem. B* **2011**, *115*, 1268–1274.

(49) Leung, M. H. M.; Kee, T. W. Effective Stabilization of Curcumin by Association to Plasma Proteins: Human Serum Albumin and Fibrinogen. *Langmuir* **2009**, *25*, 5773–5777.

(50) Gou, M.; Men, K.; Shi, H.; Xiang, M.; Zhang, J.; Song, J.; Long, J.; Wan, Y.; Luo, F.; Zhao, X.; Qian, Z. Curcumin-Loaded Biodegradable Polymeric Micelles for Colon Cancer Therapy in Vitro and in Vivo. *Nanoscale* **2011**, *3*, 1558–1567.